



An experimental investigation on the effect of relative waviness on performance of minichannel heat sinks using water and nanofluids

A. Dominic^{1,3} · V. S. Devahdhanush^{2,3} · S. Suresh³

Received: 28 July 2020 / Accepted: 31 May 2021 / Published online: 3 July 2021
© The Author(s), under exclusive licence to Springer-Verlag GmbH Germany, part of Springer Nature 2021

Abstract

An experimental investigation was conducted to study the effect of relative waviness (amplitude-to-wavelength ratio) on heat transfer and pressure drop characteristics of wavy minichannel array heat sinks. Hydrodynamically fully developed flows of de-ionized (DI) water, and 0.5% and 0.8% concentrations of Al_2O_3 /water nanofluid were introduced into two heat sinks, each with an array of 15 rectangular wavy minichannels of amplitude-to-wavelength ratio of 0.100 and 0.133. The minichannels had a width of 0.9 mm and a depth of 1.3 mm and were machined on a $30 \times 30 \text{ mm}^2$ Aluminum substrate of 11 mm thickness. Reynolds number was varied from 700 to 2300 and a constant heat flux of $45,000 \text{ W/m}^2$ was applied. Analysis of experimental results suggests increases in both Nusselt number and pressure drop with an increase in relative waviness in the laminar and transitional flow regimes. A maximum performance factor (PF) of 2.6 is achieved for a Reynolds number of 1900 using DI water in the wavy minichannels of higher relative waviness. Temperature distributions and new Nusselt number correlations for both geometries are also presented.

Abbreviations

a	Amplitude of wavy minichannel (m)
A_w	Total heat transfer area (m^2)
C_p	Specific heat capacity ($\text{J} \cdot \text{kg}^{-1} \cdot \text{K}^{-1}$)
D_{cf}	Constrictive hydraulic diameter (m)
D_h	Hydraulic diameter (m)
DI	De-ionized water
DLS	Dynamic light scattering
e	Channel height (m)
f	Fanning friction factor (-)
h	Heat transfer coefficient ($\text{W} \cdot \text{m}^{-2} \cdot \text{K}^{-1}$)
I	Heater current input (A)
j	Colburn j-factor (-)
k	Thermal conductivity ($\text{W} \cdot \text{m}^{-1} \cdot \text{K}^{-1}$)

L	Channel length (m)
m	Mass flow rate ($\text{kg} \cdot \text{s}^{-1}$)
Nu	Nusselt number (-)
P	Pressure (Pa)
PF	Performance factor (-)
Pr	Prandtl number (-)
Q	Electric power supplied (W)
q	Actual heat gain by fluid (W)
Re	Reynolds number (-)
St	Stanton number (-)
T	Temperature ($^{\circ}\text{C}$)
u	Channel bulk velocity ($\text{m} \cdot \text{s}^{-1}$)
w_c	Channel width (m)
w_{fin}	Average fin thickness (m)
ρ	Density (kg/m^3)
μ	Dynamic viscosity ($\text{N} \cdot \text{s}/\text{m}^2$)
α_c	Minichannel aspect ratio (-)
ΔP	Pressure drop (Pa)
ε	Surface roughness (μm)
ϕ	Volume concentration (-)
λ	Wavelength of minichannel (m)
app	Apparent
c	Channel
f	Fluid
meas	Measured
nf	Nanofluid
p	Plenum

✉ A. Dominic
dominic.a@sonatech.ac.in
V. S. Devahdhanush
devahdhanush@hotmail.com
S. Suresh
ssuresh@nitt.edu

¹ Department of Mechanical Engineering, Sona College of Technology, Salem 636 005, India

² School of Mechanical Engineering, Purdue University, West Lafayette, IN 47907, USA

³ Department of Mechanical Engineering, National Institute of Technology, Tiruchirappalli 620 015, India

s	Nanoparticles
sub	Substrate
st	Straight
w	Wall
x	Local

1 Introduction

In recent times various heat-dissipating devices, particularly electronic components, have been undergoing miniaturization resulting in increased power densities. Thermal management of these devices is of vital concern as accumulated heat reduces their lifetime and performance. Traditional techniques of cooling using fans and fins are unable to effectively remove the generated heat. In 1981, Tuckerman and Pease [1] proposed using mini and micro channels to obtain higher heat transfer rates. And soon after, many researchers followed suit and conducted various experiments and numerical simulations to increase the heat transfer performance of mini and micro channels. Past research works on straight mini and micro channels have concluded that conventional theories are applicable for water flow through them in the thermally developing regime when entrance region effects are also included [2]. From the work of Rao and Khandekar [3], it is known that simultaneously developing flow of water provides very high heat transfer coefficients in the entrance region. Transition from laminar to turbulent regimes was seen in the Reynolds number range of 800–1500 due to channel roughness. Similarly, hydrodynamically fully developed and thermally developing flows yield very high heat transfer coefficients in the entrance region [4]. The size of channels also affects heat transfer rate. For example, in the thermally developing laminar regime, heat transfer coefficient increases with decreasing channel size. An important point to note is that conventional correlations are unable to predict heat transfer in microchannels accurately due to mismatches in both boundary and inlet conditions between microchannels and conventional channel experiments [5].

After Choi and Eastman [6] showed an anomalously high thermal conductivity of nanofluids made by distributing metallic or non-metallic nanoparticles in water or ethylene glycol when compared to pure liquids, attention has been paid to utilize nanofluids to enhance heat transfer in mini and microchannels. This anomalous increase in thermal conductivity of nanofluids with decrease in nano particle size was studied by Koblinski et al. [7] who proposed four possible explanations: Brownian motion of molecules, molecular level layering of liquid at liquid/particle interface, nature of heat transport by nanoparticles, and nanoparticle clustering effects. They showed that the ballistic, rather than the

diffusive nature of heat transport by nanoparticles combined with direct or fluid-mediated clustering effects that provide paths for heat transport are key factors in understanding the thermal properties of nanofluids.

This heat transfer enhancement by using nanofluids has been demonstrated by many researchers. Ho et al. [8] performed experiments to investigate forced convective heat transfer coefficient of a copper microchannel heat sink with 1% or 2% vol. Al_2O_3 /water nanofluids. Jung et al. [9] measured convective heat transfer coefficient and friction factor of Al_2O_3 /water nanofluids in rectangular microchannels using various particle concentrations and found that the convective heat transfer coefficient of 1.8% nanofluid in laminar flow regime was 32% higher than that of water without major friction loss. Addition of Al_2O_3 nanoparticles to water at 4% volume fraction enhances thermal conductivity by 11.98% but dispersion of TiO_2 in water enhances the same by only 9.97%. It was found that using nanofluids such as Al_2O_3 /water and TiO_2 /water instead of water in a copper microchannel, improved cooling rates by 2.95% to 17.32% and 1.88% to 16.53%, respectively [10]. But increasing the concentration of nano particles beyond a certain limit does not necessarily increase heat transfer performance in mini and microchannel heat sinks. This was experimentally demonstrated by Sahin et al. [11], who measured steady state turbulent convective heat transfer characteristics of 0.5%, 1%, 2% and 4% Al_2O_3 /water nanofluids inside a circular aluminum tube and found that adding nano particles to pure water increased heat transfer for cases in which particle volume concentrations were lower than 2%. Also, the highest heat transfer enhancement was achieved at $Re = 8000$ and 0.5% concentration. A similar conclusion was given by Lee and Mudawar [12] that higher single-phase heat transfer coefficients are achieved in the entrance region of microchannels with increased nanoparticle concentration, but the enhancement was weaker in the fully developed region. For laminar flows in minichannels, nanofluids typically exhibit extended entrance region effects due to flattening of velocity profile caused by flow induced particle migration. Also, the onset of transition to turbulence is delayed. The friction factor and convective heat transfer coefficient of nanofluids in the transitional regime are lower than the base fluid at similar conditions. But these differences diminish in the turbulent flow regime [13].

Although straight minichannels provide better heat transfer coefficients than conventional-sized macrochannels, further improvements are possible. A geometrical modification that enhances heat transfer performance of minichannels is to use wavy channel geometries instead of straight ones. This was experimentally demonstrated by Rush et al. [14] for laminar flows in conventional-sized wavy passages. As Reynolds number was increased, the

location of onset of heat transfer enhancement moved closer to the channel entrance. At high enough Reynolds numbers, heat transfer enhancement due to the geometry of wavy channels interacted with that due to normal flow development effects [14]. Laminar flow in a wavy channel has a steady two-dimensional structure but turbulent flow has a three-dimensional vortical structure. In particular, the flow field in a large recirculation vortex within the furrow of a wavy wall shows an intermittent reversed flow and a non-uniformity of flow in the span wise direction for turbulent flows [15]. Liquid flow past bends is characterized by formation of Dean vortices along the flow direction, leading to chaotic advection, which greatly enhances mixing and heat transfer. An increase in Reynolds number results in flow transition from a steady state to periodic with a single frequency, and subsequently to a quasi-periodic flow with two incommensurate fundamental frequencies. Within these unsteady regimes, flow is characterized by very complex Dean vortex patterns which evolve temporally and spatially along the flow direction, occasionally leading to a loss in flow symmetry. Sui et al. [16] numerically simulated fully developed flow in periodic wavy rectangular channels in both steady and transitional flow regimes and supported this theory of a better heat transfer performance by wavy microchannels than straight. This was validated by their experimental study [17] of DI water flows through sinusoidal rectangular microchannels where the pressure drop penalty of wavy microchannels was found to be much smaller than their heat transfer enhancement. They also numerically studied [18] laminar flow and heat transfer of water in three-dimensional wavy microchannels with a rectangular cross section and concluded a higher heat transfer performance is possible by increasing relative waviness along the flow direction.

Our past experimental research works have established the augmented performance of minichannels over conventional sized channels, wavy minichannels over straight minichannels [19] and divergent flow passages over constant cross-section channels [20, 21] using both water and nanofluids. There is still a problem of uneven temperature distribution in heat sinks and electronic components. Although the use of wavy channels improves heat transfer performance, more amounts of heat must be removed from these locally hotter regions or “hotspots”. Locally modifying the wavy minichannel geometry with an increased relative waviness (amplitude-to-wavelength ratio, a/λ) is proposed to tackle this issue. In this study, an attempt is made to experimentally investigate the heat transfer and pressure drop characteristics of two wavy minichannel array heat sink geometries with different a/λ ratios using DI water and 0.5% and 0.8% vol. concentration Al_2O_3 /water nanofluids in both laminar and transitional flow regimes.

2 Formulation of nanofluid

2.1 Preparation

Two volume concentrations (0.5% and 0.8%) of nanofluids were prepared by dispersing commercial α -phase Al_2O_3 nano particles (NanoDur 99.5%, Alfa Aesar, India) in DI water following the two-step method [22]. The nominal diameter of these nano particles is 40 nm (the minimum and maximum diameters being 37.6 nm and 44.4 nm respectively) and a Scanning Electron Microscopy (SEM) image of these nano particles before dispersion is shown in Fig. 1. The prepared solutions were sonicated by an ultrasonic vibrator (40 kHz, Lark, India) which generated ultrasonic pulses of 180 W at 40 kHz for 60 min.

2.2 Study of quality and stability of prepared nanofluids

Even though nanofluids have potential features of heat transfer enhancement, improper methods of preparation and usage might lead to problems such as agglomeration, sedimentation, and degradation of thermo-physical properties. To assess both the quality and stability of the prepared nanofluids, their particle size distribution, Zeta potential distribution, and pH factor were investigated [23, 24].

The size of dispersed nanoparticles in water was measured using a Zetasizer (Nano ZS, Version 7.01, MAL1045544, Malvern Panalytical, UK) and the size distribution report is shown in Fig. 2. Measurement is done by Dynamic Light Scattering (DLS), a technique which employs a correlation between the rate of intensity fluctuation of light scattered by

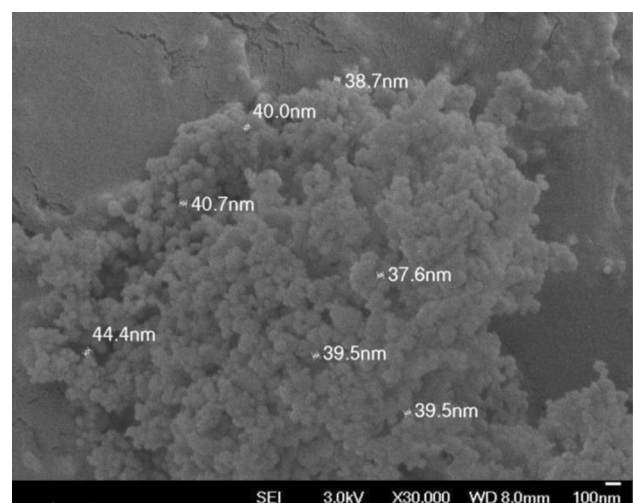
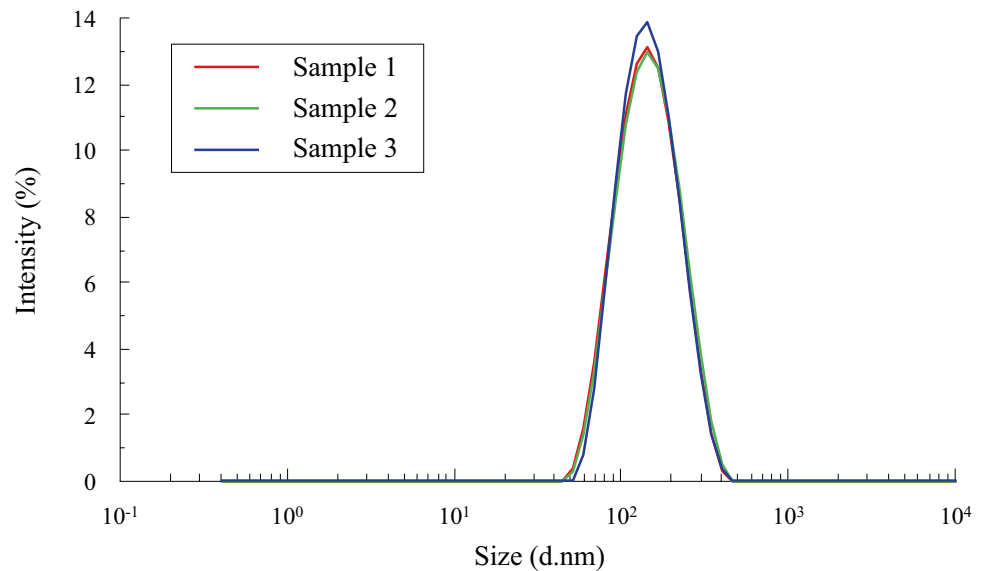


Fig. 1 Scanning Electron Microscopy (SEM) image of Al_2O_3 nanoparticles prior to dispersion in DI water

Fig. 2 Size distribution by intensity of nano particles in 0.8% Al₂O₃/water nanofluid (3 samples)

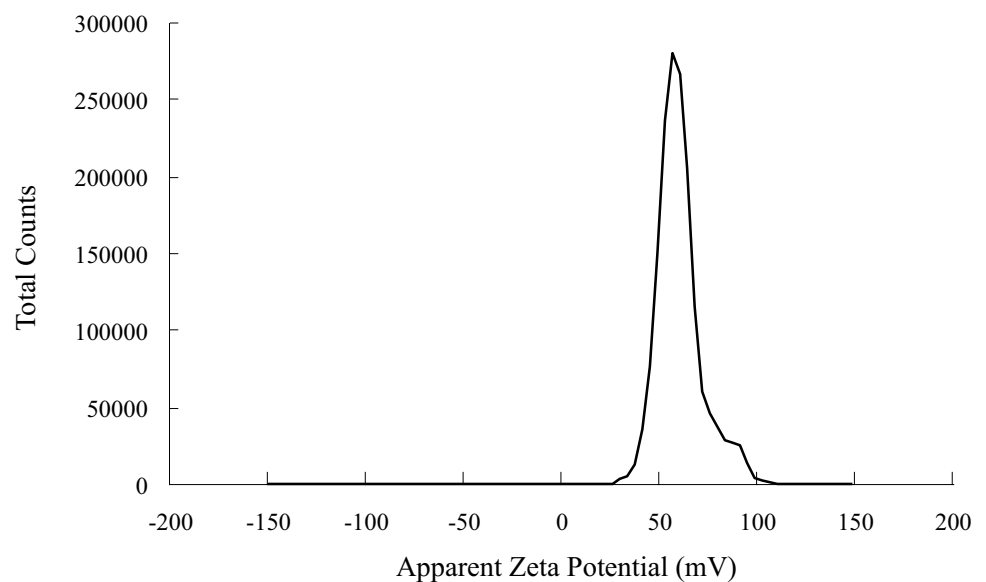


sub-micron sized particles and their size [25]. This intensity fluctuation is due to the different speeds at which various particles are undergoing Brownian motion. Smaller particles cause more rapid intensity fluctuations than the larger ones, but larger particles and samples of high concentrations scatter more light [24]. The result of DLS is not the actual size of each particle by itself, but rather the hydrodynamic particle diameter which depends on size of particle before dispersion, size of any surface structures, and the type and concentration of any ions present in the nanofluid. As evident from Fig. 2, the average hydrodynamic diameter of dispersed nanoparticles is 131 nm for three different samples. This value is slightly higher than the actual average diameter of nanoparticles from Fig. 1, suggesting a slight amount of particle agglomeration and clustering. Since both

the hydrodynamic and actual diameters of the particles are close to one another, the dispersion quality is considered good and the nanofluid is deemed stable.

The Zeta potential of the prepared nanofluids was measured using a Zetasizer (Nano ZS, Version 7.01, MAL1045544, Malvern Panalytical, UK) and a statistical distribution of the apparent Zeta potential is shown in Fig. 3. Zeta potential or electrokinetic potential of nanofluids is the electrical potential difference between dispersion medium (DI water) and stationary liquid layer attached to nanoparticles. Nanofluid stability is indicated by the magnitude of Zeta potential, where values higher than 60 mV indicate an excellent electrical stability, 30–60 mV indicate a good stability, and those lower than 30 mV indicate the beginning of dispersion [24, 26]. At these low or near-zero values

Fig. 3 Zeta potential distribution of nano particles in 0.8% Al₂O₃/water nanofluid



(near the iso-electric point), particle settlement is caused by weaker repulsive forces that are unable to overcome the attractive van der Waals forces between different particles and the prepared nanofluid separates into different layers. Figure 3 shows that the Zeta potential of prepared nanofluids at a temperature of 25 °C is 60.8 mV with a Zeta deviation of 9.04 mV, indicating a good-to-excellent stability.

For a stable solution of nanofluids, the value of pH should be away from its iso-electric point (IEP). The IEP of Alumina nanoparticles is 9.2 [27]. Even though nanofluids can be stabilized by maintaining their pH by the addition of certain surfactants or pH changers, this may affect their effective thermal conductivity [28]. Al₂O₃/water nanofluids were prepared without adding any surfactant and their pH value was measured using a pH meter (Model 111/101, Deep Vision) to be around 8, an indication of stability.

2.3 Evaluation of properties

The thermo-physical properties of nanofluids were calculated at their average bulk temperature [20]. The density, thermal conductivity, and specific heat capacity of the nanoparticles are $\rho_s = 3.6$ g/cc, $k_s = 76.5$ W/m-K, and $C_{p,s} = 880$ J/kg-K, respectively. Since the highest volume concentration of nanoparticles used in this study was 0.8%, the density of Al₂O₃/water nanofluid was determined by using Pak and Cho's [29] Eq. (1) and the dynamic viscosity was calculated by using the viscosity correlation (2) proposed by Einstein [30] as

$$\rho_{nf} = (1 - \phi)\rho + \phi\rho_s \quad (1)$$

and

$$\mu_{nf}(1 + 2.5\phi)\mu \quad (2)$$

This is consistent with Suresh et al. [23], and Jang and Choi [31]. The specific heat capacity of nanofluids was calculated using Xuan and Roetzel's [32] Eq. (3),

$$C_{p,nf} = \frac{(1 - \phi)\rho C_p + \phi\rho_s C_{p,s}}{\rho_{nf}} \quad (3)$$

The effective thermal conductivity of nanofluids, k_{nf} , was calculated using the Maxwell model [33]. For nanofluids with a volume fraction of less than unity, Maxwell's equation is given by (4) [23],

$$\frac{k_{nf}}{k} = \frac{k_s + 2k + 2\phi(k_s - k)}{k_s + 2k - \phi(k_s - k)} \quad (4)$$

For example, the thermophysical properties of 0.5% nanofluid at 20 °C estimated using Eqs. (1) – (4) are: $\rho_{nf} = 1011$ kg/m³, $\mu_{nf} = 0.000866$ Pa.s, $C_{p,nf} = 4119.3$ J/kg.K, and $k_{nf} = 0.595$ W/m.K.

In our previous studies [20, 23], the thermal conductivity and viscosity of prepared nanofluids were respectively measured using a KD2 Pro Thermal Analyzer and a Brookfield Viscometer and compared with theoretical values calculated using Eqs. (4) and (2). The respective differences were just between 1 and 3% for a volume concentration of 0.8% [20, 23]. Although nanofluids have favorable effects on heat transfer performance, some of their properties are undesirable such as a higher viscosity and density, and a lower heat capacity than those of the base fluid. 2.4%, 2.08% and 1.99% increases in thermal conductivity, density and viscosity, respectively, and a 2.25% decrease in specific heat capacity is seen for a 0.8% vol. concentration of Al₂O₃/water nanofluid over DI water [12, 20].

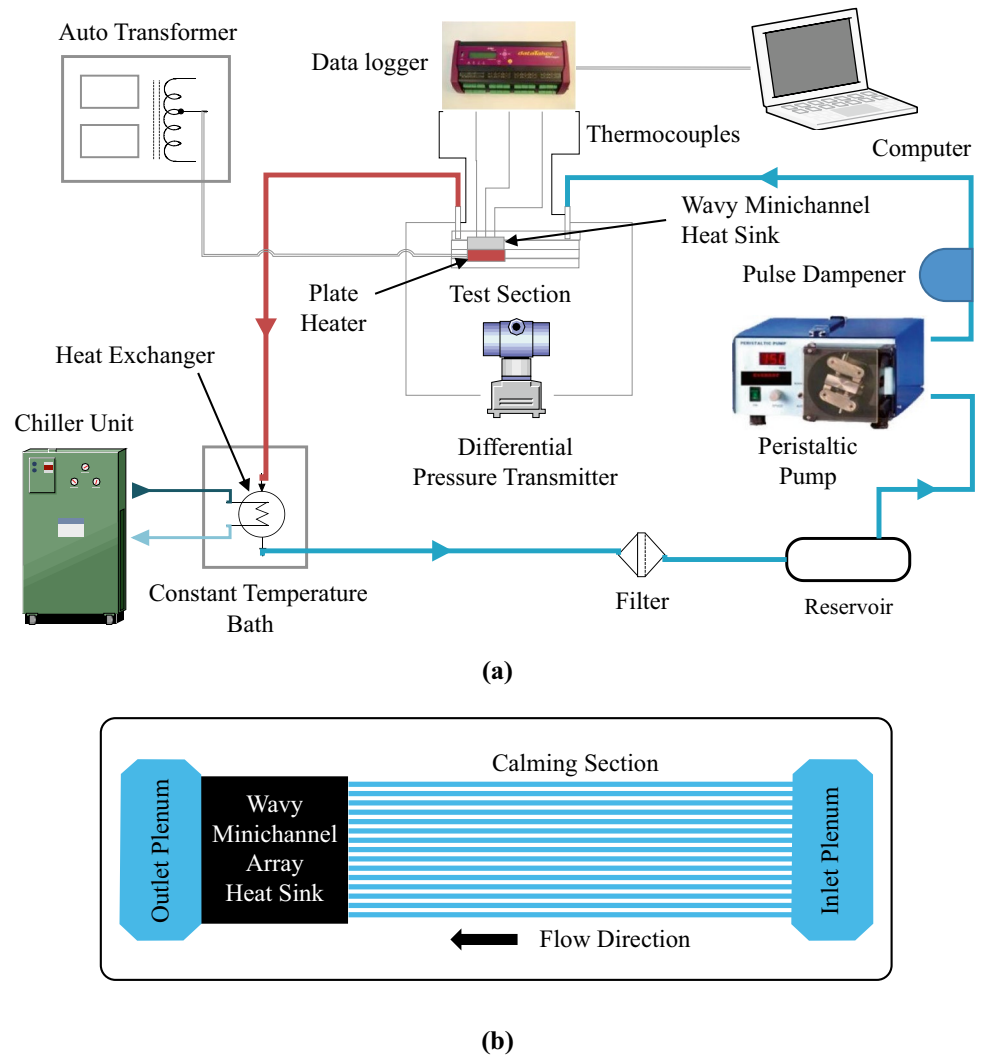
3 Experimental method

3.1 Experimental setup

A schematic representation of the experimental flow loop used in the present study is shown in Fig. 4(a). This setup has already been validated against past literature in our previous study [19]. The working fluid is drawn from a liquid reservoir by a peristaltic pump (4 l/min, RH-P120LS, Ravel Hiteks, Chennai, India), which offers two advantages: (i) fluid is positively displaced in only the set direction, and (ii) fluid is kept isolated from the pumping mechanism. The latter advantage makes peristaltic pumps more suitable for nanofluids, by ensuring that nanoparticles do not interact with the moving parts. A pulse dampener is provided downstream of the pump to reduce periodic flow rate fluctuations from the peristaltic pump, especially at the lower flow rate range. This cold fluid enters the minichannel test section where it gains sensible heat from the heat sink and increases in temperature. The hot fluid rejects the acquired heat in a heat exchanger, which is placed in a constant temperature bath. A chiller unit helps maintain a constant bath temperature, and therefore a constant fluid temperature at the test section inlet. Fluid from the heat exchanger then passes through a filter where any possible impurities are removed, and thereafter to a reservoir. The filter size was chosen to be bigger than the nanoparticle size. For the duration of all experiments, since prepared nanofluids were stable without any significant particle clustering and agglomeration, the filter did not cause any blockages or negatively affect fluid flow.

The most important components of the heat sink test section include the minichannel heat sink, plate heater, and housing. Detailed technical drawings of the two heat sink geometries used in this study are shown in Fig. 5. Both the heat sinks were machined out of 11-mm-thick Aluminum plates of 30 × 30 mm² cross-sectional area. An array of 15

Fig. 4 Schematic representations of (a) experimental setup and (b) flow path within experimental test section

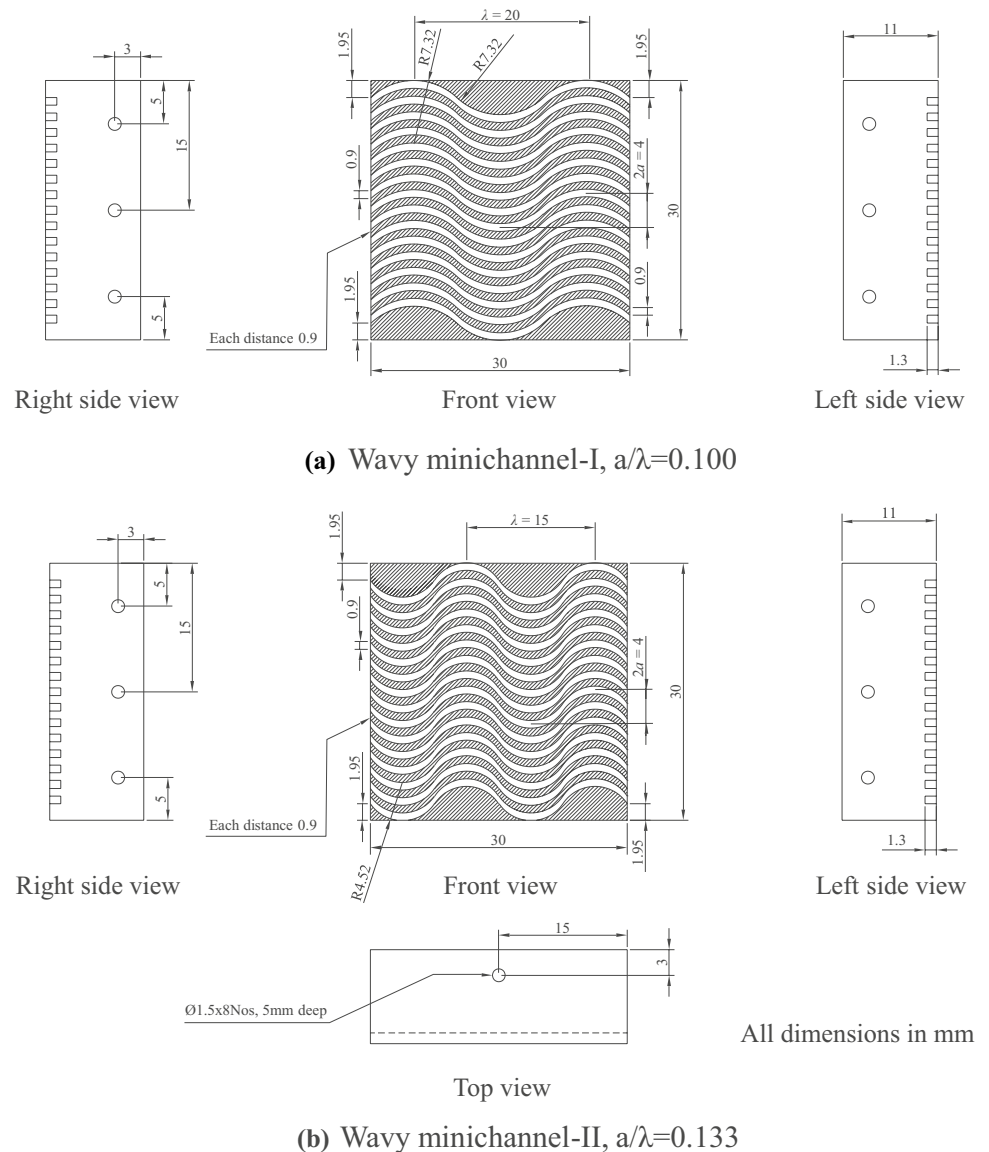


wavy minichannels were made on the top heat sink surface by Computerized Numerical Control (CNC) milling. Each wavy channel has a height of $e = 1.3$ mm, width of $w_c = 0.9$ mm, hydraulic diameter of $D_h = 1.063$ mm and aspect ratio of $\alpha_c = 1.444$. The average fin thickness, w_{fin} , is maintained equal to the channel width, w_c . Note that practical machining of these heat sinks causes only the channel width to be constant all along the channel length, but the fin thickness to vary slightly along its length. The only parameter that is different for the two heat sinks is relative waviness, a/λ , of channels, based on which they are designated as wavy minichannel-I for $a/\lambda = 0.100$, and wavy minichannel-II for $a/\lambda = 0.133$, as shown in Figs. 5(a) and 5(b), respectively. Note that both geometries have the same amplitude, $a = 2$ mm, but different wavelengths, $\lambda = 15, 20$ mm. After machining, the surface roughness, ϵ , of channel walls was measured using a surface profilometer to be $40.94 \mu\text{m}$. Both heat sinks have provisions for placing eight thermocouples for substrate temperature measurement, by

means of 1.5-mm-diameter and 5-mm-deep holes drilled 6.7 mm below the bottom wall of channels. Three, two, and three of these eight substrate thermocouples measure the substrate temperature 5, 15, and 25 mm downstream from the inlet, respectively. This helps gain an understanding of heat sink temperature distribution. Heat is supplied to the bottom of heat sinks by a resistance plate heater of size $50 \text{ mm} \times 50 \text{ mm} \times 5 \text{ mm}$. Thermal grease of conductivity, 8.7 W/m.K , is applied to the solid–solid interface between them to reduce thermal contact resistance. Variable AC power is supplied by an auto transformer and the voltage and current values are recorded.

The test section housing is made of four plates of polycarbonate, which was chosen for its low thermal conductivity (0.2 W/m.K) and transparency. Both inlet and outlet manifolds are fitted on to the top housing plate and have provisions for K-type thermocouples and a differential pressure transmitter (M94-DP65L, ABUS Technologies) to measure the inlet and outlet fluid temperatures and pressure drop

Fig. 5 Technical drawings of both heat sinks: (a) wavy minichannel-I, $a/\lambda=0.100$ and (b) wavy minichannel-II, $a/\lambda=0.133$



respectively. Average fluid temperatures in the test section were measured to be in the range of about 27 °C to 31 °C. The second plate houses the inlet and outlet plenums, the heat sink and a calming section machined on it, and the entire fluid path within the test section is between the top and second housing plates. Figure 4(b) illustrates the flow path within the minichannel test section. Both plenums are 25% wider on either side of the heat sink with a 45° inclination for even flow distribution through all channels [2]. Fluid entering the test section from the inlet manifold is collected in the inlet plenum, from which it enters a calming section made of 15 long minichannels of the same cross-sectional area and spacing as the heat sink. The purpose of this calming section is to ensure a hydrodynamically developed and thermally developing flow at the minichannel heat sink inlet for a higher heat transfer rate. The Nusselt number of

thermally developing flow is higher than fully developed flow because of the larger temperature gradient for thinner thermal boundary layer; typically, the thinner the boundary layer, the larger the heat transfer coefficient. The hydrodynamic boundary layer starts developing from the inlet of the calming section and becomes developed after crossing the hydrodynamic entrance length, which is less than the total length of the calming section. Heating of fluid starts at the heat sink inlet and the thermal boundary layer starts developing there, but never becomes fully developed since the heat sink minichannel length was kept shorter than the thermal entrance length. Since the thermal conductivity of top polycarbonate wall is low, it can be assumed to be an adiabatic wall. The heat transfer boundary condition is three-sided heating with constant heat flux from the bottom of the channel. The third and fourth housing plates help keep the

plate heater in place. The housing is made leak proof by using an RTV sealant (Anabond Silicon Red), and the entire test section is placed inside a wooden box filled with highly insulating glass wool to reduce heat leaks to ambient.

3.2 Test procedure

For a heat sink and fluid combination, the heat flux and flow rate are respectively set by adjusting autotransformer brush position and rotation speed of peristaltic pump. Fluid and substrate temperatures, that are measured using a datalogger (DT85 Data Taker, Thermo Fisher Scientific, Scoresby, Australia), are monitored. After the system reached steady state conditions (which approximately took 60 min for each case), temperature readings are recorded in the datalogger at a frequency of 5 Hz and pressure drop readings are recorded from the differential pressure transmitter display. A mean of at least 100 readings is considered as the steady state value. This process is repeated for other flow rates, heat sink, and fluid combinations.

3.3 Data processing

The hydraulic diameter of rectangular minichannels is calculated as

$$D_h = \frac{2w_c e}{w_c + e} \quad (5)$$

Since surface roughness affects flow and heat transfer to a considerable extent in minichannels [34], constrictive hydraulic diameter given by Eq. (6) is used in all calculations and the corresponding Reynolds number can be calculated using Eq. (7).

$$D_{cf} = D_h - 2\epsilon \quad (6)$$

$$Re = \frac{\rho u D_{cf}}{\mu} \quad (7)$$

The power, Q , supplied by the auto transformer to plate heater is given by Eq. (8) in terms of its output voltage, V , and supplied current, I . Even though the plate heater was covered by highly insulating Teflon on all sides except the heating surface, the fluid picked up a reduced amount of heat, q , given by Eq. (9). The difference between these two values gives the amount of heat loss to surroundings, which amounted to a maximum of 12%. For each test case, all thermo-physical properties of the working fluid are considered constant and taken at the mean fluid temperature (average of inlet and outlet temperatures).

$$Q = VI \quad (8)$$

$$q = mC_p \Delta T \quad (9)$$

where ΔT is the temperature difference of working fluid between inlet and outlet. The minichannel wall temperatures are calculated from the substrate thermocouple readings, by assuming an one-dimensional conduction as\

$$T_w = T_{sub} - \frac{qL_{conduction}}{A_{sub}k_{sub}} \quad (10)$$

where $L_{conduction}$ is the distance between thermocouples and channel bottom. Local wall temperatures at three axial locations (5 mm, 15 mm, and 25 mm from inlet) are determined by averaging the lateral values. The applied heat flux being uniform and heat transfer being solely by single-phase convection, by energy balance, fluid temperatures at these three axial locations are estimated by a linear interpolation between the inlet and outlet fluid temperatures. Both local heat transfer coefficients and local Nusselt numbers at these three axial locations are respectively determined as

$$h_x = \frac{q}{A_w(T_w - T_f)} \quad (11)$$

and

$$Nu_x = \frac{h_x D_{cf}}{k_f} \quad (12)$$

where A_w is the total convective area of all minichannels in each heat sink. Since the three axial locations are equally spaced along a line, average heat transfer coefficients and Nusselt numbers is determined by a simple arithmetic average of the three local values.

From the experimentally measured pressure drop, the apparent pressure drop (excluding losses) and the apparent friction factor are calculated using

$$\Delta P_{meas} = \frac{\rho u^2}{2} \left[2k_{90} \left(\frac{A_c}{A_p} \right)^2 + (k_c + k_e) + \frac{4f_{app}L}{D_{cf}} \right] \quad (13)$$

and

$$f_{app} = \frac{\Delta P_{app} D_{cf}}{2\rho Lu^2} \quad (14)$$

where k_{90} , k_c and k_e are loss coefficients due to 90° bends, inlet contraction and outlet expansion area changes respectively. k_{90} is approximately 1.2, and k_c and k_e are taken from the tables of Kays and London [40] and Phillips [41]. For the Reynolds number range of 700 – 2300, k_c varies from 0.7 to 0.45 and k_e varies from 0.05 to 0.2 [40, 41]. A list of

values/ranges of important experimental parameters of this study is included in Table 1.

3.4 Experimental uncertainties

Uncertainty analysis was done to find the influence of experimental parameters on various measurement variables [20, 35] by following the Coleman and Steele method [36] and ANSI/ASME standard [37]. The maximum uncertainties in the measurement of temperature (in °C), pressure drop (in Pa) and mass flow rate (in kg/s) are 3.40%, 10.90% and 0.58%, respectively. The maximum uncertainties in Nusselt number, Reynolds number, and Fanning friction factor are calculated to be 11.37%, 3.58%, and 18.06%, respectively.

4 Results and discussion

Experimental results of two wavy minichannels with different a/λ ratios of 0.100 (wavy minichannel-I) and 0.133 (wavy minichannel-II), using DI water and Al_2O_3 /water nanofluid as working fluids are considered for discussion.

4.1 Heat transfer rate of wavy channels

4.1.1 Effect of wavy geometry

The three main contributors to heat transfer augmentation in wavy minichannels are: (i) conventional effects of minichannels [19], (ii) wavy geometry effects, and (iii) increased heat transfer surface area for the same heat sink base footprint [20, 21]. The smaller hydraulic diameter of minichannels compared to conventional-sized macrochannels increases fluid contact with channel walls and a larger entrance effect; the latter due to a higher relative

surface roughness resisting boundary layer development. The wavy geometry contributes to the production of Dean vortices at the troughs of each wave, which leads to more fluid mixing and disturbs the core flow development. Wavy channels are also longer than straight channels, leading to a longer residence time of fluid within the channels. The total heat transfer surface area within the heat sink is increased by both the above-mentioned geometrical factors: minichannels and wavy geometry. The variation of Nusselt number, Nu , with Reynolds number, Re , is shown in Fig. 6, where the lower set of curves correspond to wavy channel-I and the upper set of curves to wavy channel-II. The wavy channel-I curves follow a similar constant slope up to $Re \approx 1900$. This region corresponds to laminar flow regime, where Nu monotonically increases with increasing Re .

When fluid passes through wavy passages particularly at the crests and troughs, secondary vortices or Dean vortices [15, 18] are formed that enhances stretching and folding of flow elements causing fluid mixing and chaotic advection. This mixing disturbs the hydrodynamic and thermal boundary layers and reduces their thickness. Hence, the average heat transfer rate is enhanced while the temperature gradient of flowing fluid is reduced. This effect can be observed in the curves of temperature distribution as function of distance along the streamwise direction, as shown in Fig. 7. The Nusselt number of flows through wavy channel-I in the laminar regime can be predicted using the correlation,

$$Nu_{\text{wavy-I}} = 0.8204Re^{0.274}Pr^{0.33}(1 + \phi)^{14.8974} \quad (15)$$

within an error range of -6.134% to 3.575%. From Eq. (15), it is inferred that the effect of Prandtl number on Nusselt number is similar to standard correlations [38]. But the effect of Reynolds number on Nusselt number was significant, because it affected flow properties by producing vortices and increased mixing. The effect of volume fraction of nano particles in laminar regime is better than that in the transitional regime, because their effects in the latter regime are suppressed by the onset of turbulence [13].

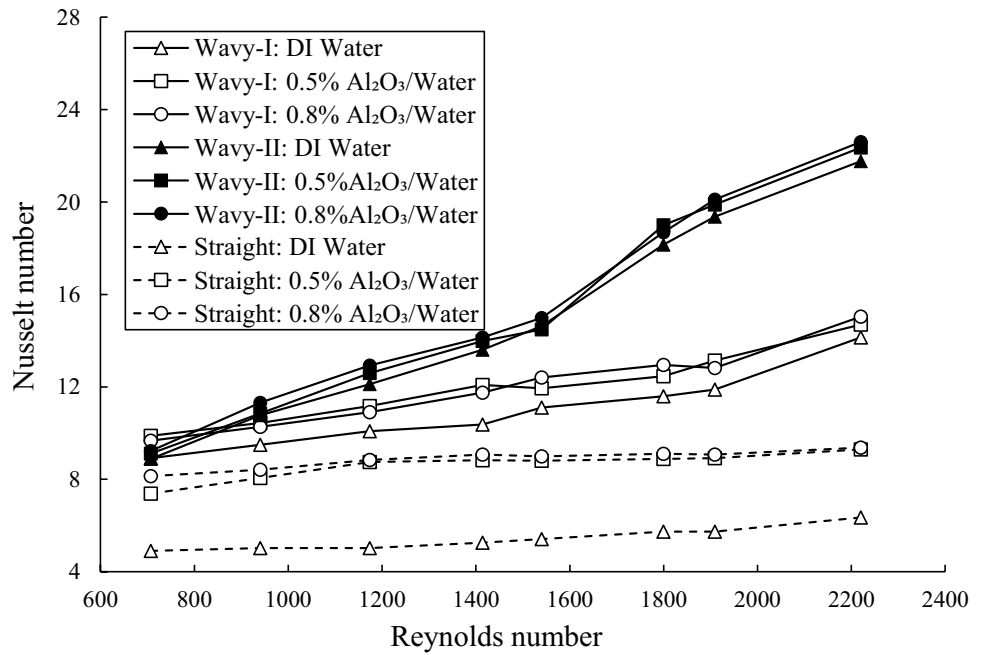
The second part of the same curves in Fig. 6 shows a larger Nu dependence on Re in the transitional and early parts of turbulent regimes compared to laminar. In transitional flow, stretching and folding of vortices causes longitudinal vortices where the flow becomes three dimensional. Further increase in Reynolds number increases mixing and the three-dimensionality spreads to all other regions [15]. Transition starts around $Re \approx 1900$, which can also be seen in Fig. 9 where friction factor keeps on decreasing up to $Re \approx 1900$, and then starts increasing.

The upper set of curves in Fig. 6, that correspond to wavy channel-II, show similar trends, but the slopes and transition points are different. Laminar flow is maintained until $Re \approx$

Table 1 Values/Ranges of Experimental Parameters

Parameter	Value/Range
Flow rate	$(0.656 - 2.059) \times 10^{-5} \text{ m}^3/\text{s}$
Flow velocity, u	0.576 – 1.809 m/s
Reynolds number, Re	707 – 2220
Voltage, V	97 V
Current, I	0.414 A
Heat input, Q	~ 40 W
Nusselt number, Nu	8.88 – 22.60
Pressure drop, ΔP	2043 – 21,127 Pa
Fanning friction factor, f	0.059 – 0.122
Colburn j-factor, j	$(3.35 - 7.77) \times 10^{-3}$
Performance factor, PF	0.909 – 2.685

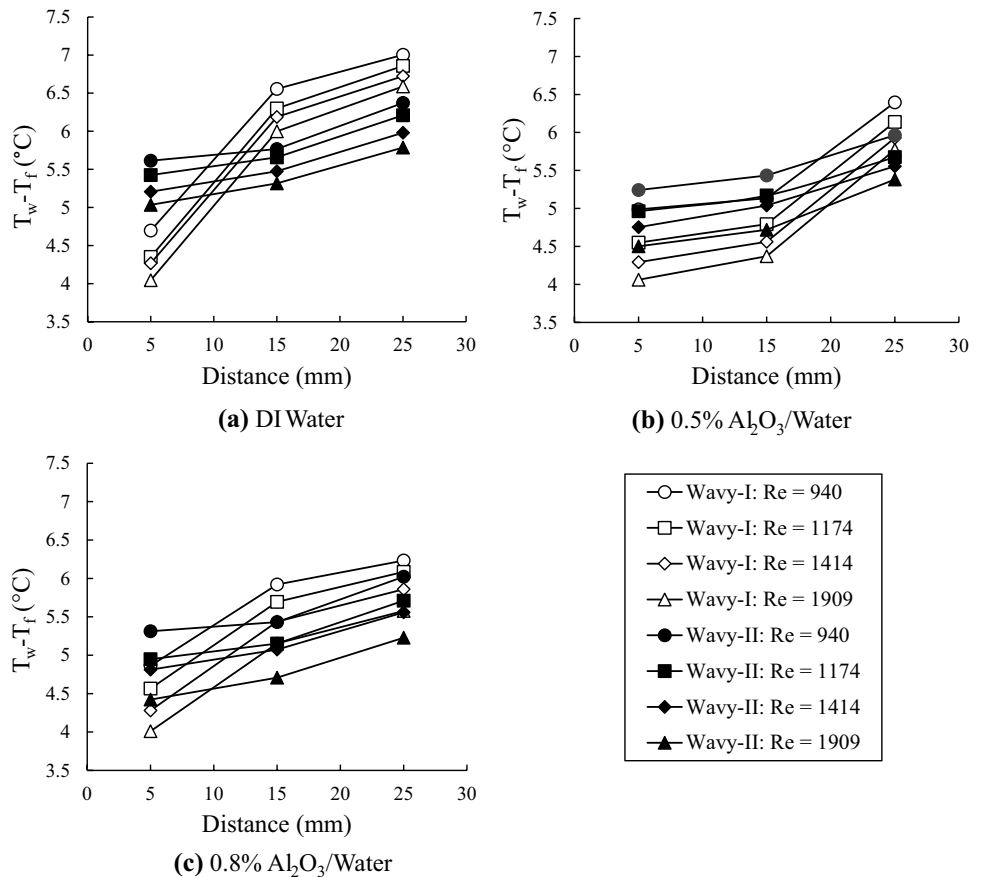
Fig. 6 Nusselt number variation with Reynolds number for DI water and nanofluids in both channel configurations (Wavy-I: $a/\lambda=0.100$, Wavy-II: $a/\lambda=0.133$). Straight channel configuration data is included for reference



1540, evidenced by Nu slope change and also a change in slope of friction factor. Transitional Re of Wavy channel-II is slightly lower than Wavy channel-I due to higher relative

waviness. The Nusselt number of flows through wavy channel-II in the laminar regime can be predicted using the correlation,

Fig. 7 Wall temperature distribution along the axial direction for (a) DI water, (b) 0.5% Al_2O_3 /water nanofluid and (c) 0.8% Al_2O_3 /water nanofluid (Wavy-I: $a/\lambda=0.100$, Wavy-II: $a/\lambda=0.133$)



$$Nu_{\text{wavy-II}} = 0.092Re^{0.616}Pr^{0.30}(1 + \phi)^{5.742} \quad (16)$$

within an error range of -1.672% to 4.056%. We can observe from Eq. (16) that the effect of Pr on Nu is almost the same as Eq. (15) and Dittus-Boelter correlation [38] because the variation in fluid properties in the present study is less. But the effect of flow properties (i.e. Re) on Nu is higher because the channel wavy geometry creates turbulence and chaotic mixing [15, 17, 18].

A 3 to 32% higher Nu is observed for Wavy-II over Wavy-I in laminar regime and a maximum Nu enhancement of 63% at $Re \approx 1900$ in the transitional regime. This is due to more secondary vortices, circulation, separation, and attachment to the core flow [16–18].

4.1.2 Effect of nanofluids

Figure 6 also shows the effects of using nanofluids over DI water in both wavy channels. In the laminar regime of wavy channel-I, there is a 7% to 21% enhancement in Nusselt number for 0.5% Al_2O_3 /water and a 5% to 21% enhancement for 0.8% Al_2O_3 /water over DI water. This is due to improved thermo-physical properties by the addition of nano particles to base fluid. In the transitional regime, Nu augmentation is 3% to 5% over DI water, at higher Reynolds numbers of $Re \approx 2200$. From these values, we can infer that the effect of nanofluid is overshadowed by the geometry of wavy channels in the transitional regime. It is noted that, in straight minichannels, nanofluids yield a rather significant improvement over DI water solely due to improved thermo-physical properties [19].

For wavy channel-II, the increase in Nusselt numbers are 3% to 4% and 4% to 7% for 0.5% and 0.8% Al_2O_3 /water compared to DI water, respectively. In the transitional regime, it is a maximum of 4% for both nanofluids due to a higher relative waviness [13]. On increasing the relative waviness, the effects of nanofluid get suppressed, which can easily be deduced by comparing the exponents on the volume concentration factor in Eqs. (15) and (16). The enhanced chaotic movement of fluid particles at the onset of turbulence in wavy channels reduces the temperature gradient of fluid. So, the effect of nanofluid on heat transfer rate in transitional regime is less than that in laminar regime and converges with DI water. The curves of variation in Nu with Re for both channels follow a similar trend. It is inferred that the effect of nanofluid on heat transfer enhancement is suppressed by the turbulence created by wavy form of channels in both laminar and transitional regimes. This is clearer in the transitional regime due to larger turbulence effects.

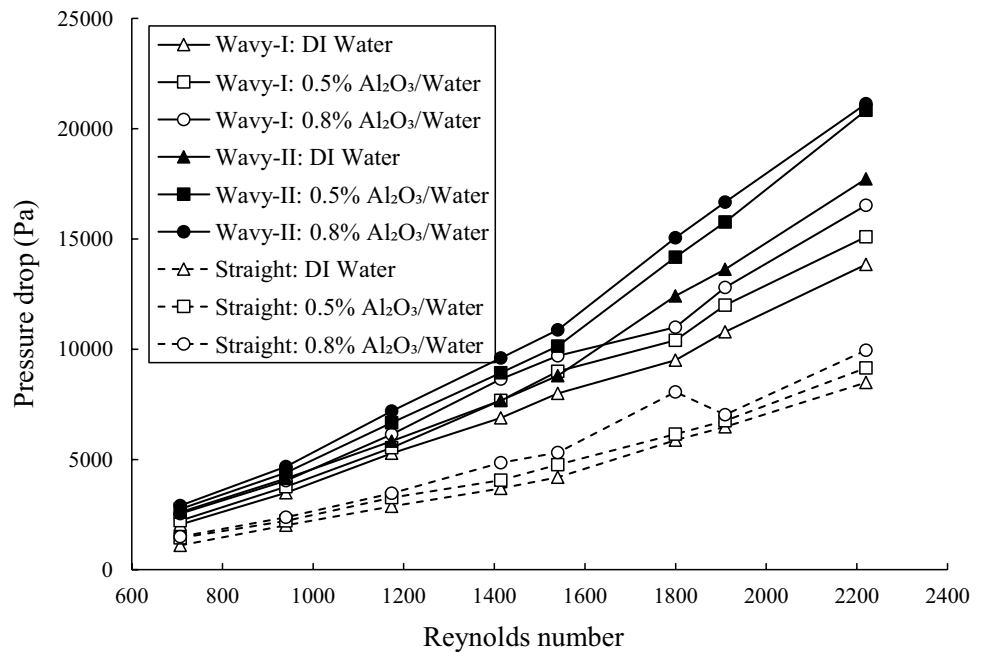
4.2 Temperature distribution of wavy minichannels

The average heat transfer coefficient or average Nusselt number is an indication of the heat transfer performance of a system. To describe the complete heat transfer performance, it is important to analyze the heat sink temperature distribution along the streamwise direction. As described in Sect. 3, wall temperature at various axial distances (5 mm, 15 mm, and 25 mm from heat sink inlet) was measured by using thermocouples. The fluid temperature at these locations was determined by a linear interpolation between the inlet and outlet fluid temperatures. The temperature difference between the wall and the fluid is calculated and plotted against axial distance as shown in Fig. 7. In general, the axial temperature of heat sink increases from inlet to outlet in a straight minichannel [18]. A significant temperature change is noticed only in the entrance region of straight minichannels. This lower temperature near the entrance reduces the average temperature of heat sink. It is inferred from Fig. 7 that the entrance effect is suppressed by the wavy geometry of channel, and a higher relative waviness gives a better temperature distribution. It is known that the average temperature of wavy minichannels is less than that of straight minichannels for the same Reynolds number [19]. The wavy geometry of a channel produces Dean vortices and they disturb boundary layer development and increase fluid mixing until the trailing end of channels. Increasing Re also increases heat transfer rate and yields a better temperature distribution. The development of secondary oscillations in the trailing end of channels at lower Re moves towards the entrance when Re is increased [39]. These are the reasons for less variation in temperature difference along the flow direction and lower average surface and fluid temperatures. Figure 7 shows that higher relative waviness yields better results because of enhanced mixing, chaotic advection, circulation and reattachment [18]. As already discussed, nanofluids yield a less significant heat transfer performance in laminar regime, which further diminishes in transitional regime. Upon increasing relative waviness, the effects of nanoparticles are curbed, and thermal performance converges to that of the base fluid [13]. An increased volume concentration of nanoparticles absorbs more heat, increases fluid temperature, and thereby reduces surface temperature. The trend of decreasing slope of curves can be seen in Fig. 7.

4.3 Pressure drop and friction factor

Besides heat transfer, other important factors in determining the performance of each heat sink are pressure drop and friction factor. It is already known that flow through minichannels incur larger pressure drop due to

Fig. 8 Pressure drop variation with Reynolds number for DI water and nanofluids in both channel configurations (Wavy-I: $a/\lambda=0.100$, Wavy-II: $a/\lambda=0.133$). Straight channel configuration data is included for reference

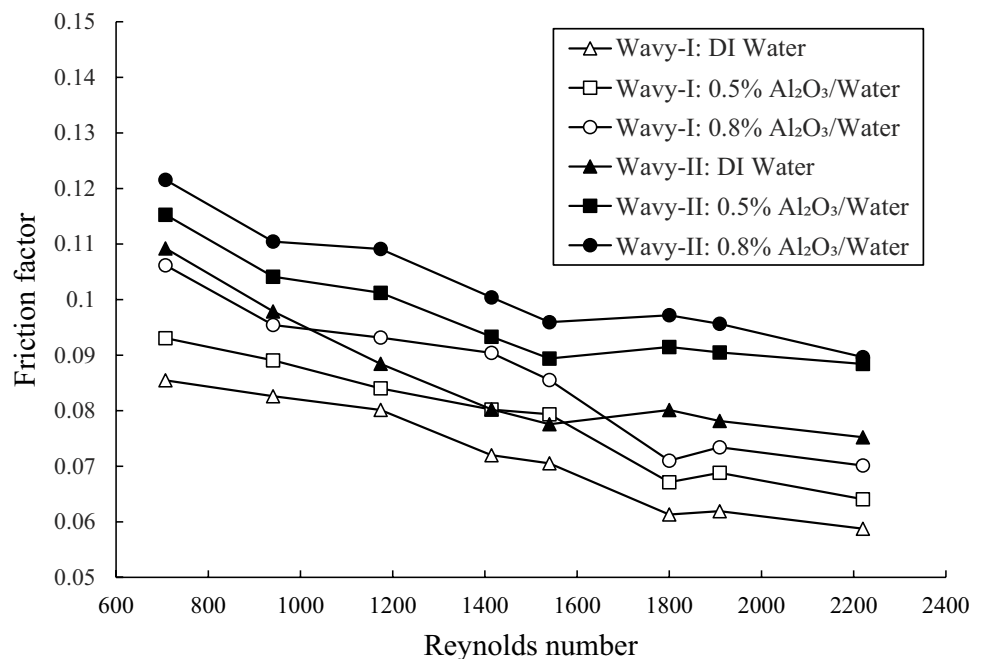


their smaller flow passages. Figure 8 shows the variation of pressure drop with Reynolds number for DI water and nanofluids in both channel geometries (Wavy-I: $a/\lambda=0.100$, Wavy-II: $a/\lambda=0.133$). The differential pressure between the inlet and outlet manifolds of test section was measured using a differential pressure transmitter for adiabatic flow. This measured pressure drop value includes pressure losses because of flow friction, bends, entrance contraction and exit expansion, and developing

region effects. The apparent friction factor [22, 40, 41] which includes just the frictional and entrance effects is calculated from the experimentally measured values using Eq. (14).

Figure 9 shows the variation of apparent friction factor with Re . Friction factor decreases with Reynolds number until a point at which flow transition occurs. Transitioning occurs around the Re range of 1500 – 2000 for wavy channel-I. This value is slightly lower than that given by

Fig. 9 Fanning friction factor variation with Reynolds number for DI water and nanofluids in both channel configurations (Wavy-I: $a/\lambda=0.100$, Wavy-II: $a/\lambda=0.133$)



conventional theories and this kind of earlier transition from laminar regime has been noticed by other researchers [3, 22, 42–45]. After this point, friction factor increases a little and then becomes fairly constant in the transitional regime. Minichannels of increased relative waviness also exhibit this trend, but the advent of transition regime is at a slightly lower Re . It is inferred from Fig. 8 that the increase in pressure drop due to increased relative waviness is less significant in laminar regime than transitional regime; this is because of smaller vortices produced at the troughs by streamlined laminar flow. But flow at high Re produces more turbulence effects leading to secondary accelerations and larger vortices that increase pressure drop. The reason for this earlier transition is stronger liquid layer mixing effects in the flow channel because of increased relative waviness and relative surface roughness.

Increasing volume concentration of nanofluid from 0% to 0.8% increases friction factor from 15 to 25% and 11% to 25% for wavy minichannels I & II, respectively, in the laminar regime due to changes in fluid properties such as density, viscosity, conductivity and surface tension, etc. In the transitional regime, the friction factor of water is almost constant, but decreases in the case of nanofluids. This could be because small particles suppress turbulence by acting as an additional source of dissipation [13]. Since 40 nm diameter nano particles are used in this study and $Re < 2300$, the particles used are considered small [46]. Changes in heat transfer trend in Fig. 6 is also seen at this same Re . So, we conclude that increasing relative waviness increases friction factor, pressure drop, and heat transfer.

4.4 Colburn j-factor

The heat transfer performance of both wavy channel heat sinks can further be presented using the Colburn j-factor, which is estimated as

$$j = St.Pr^{2/3} = \frac{Nu}{Re.Pr^{1/3}} \quad (17)$$

where St is the Stanton number. The variation of j-factor with Reynolds number in logarithmic coordinates for DI water and nanofluids in both heat sinks is shown in Fig. 10, along with the respective friction factor. Overall, friction factors for each combination of fluid and channel geometry are roughly an order of magnitude higher than the j-factors. Figure 10 also helps in easy identification of flow regime transitions [40]. It is apparent from the slope of j-factor curves that, for all fluids in Wavy-II, flow transitions from laminar to transitions regimes at $Re \approx 1540$. And for all fluids in Wavy-I, the slope changes at $Re \approx 1900$, marking

the transition in flow regimes. For a fixed channel geometry, flow regime transition is not affected by the selection of working fluid (DI water or 0.5% or 0.8% nanofluids). Similar changes in slope at around the same Reynolds numbers are seen in the friction factor curves but are less pronounced.

4.5 Overall performance factor

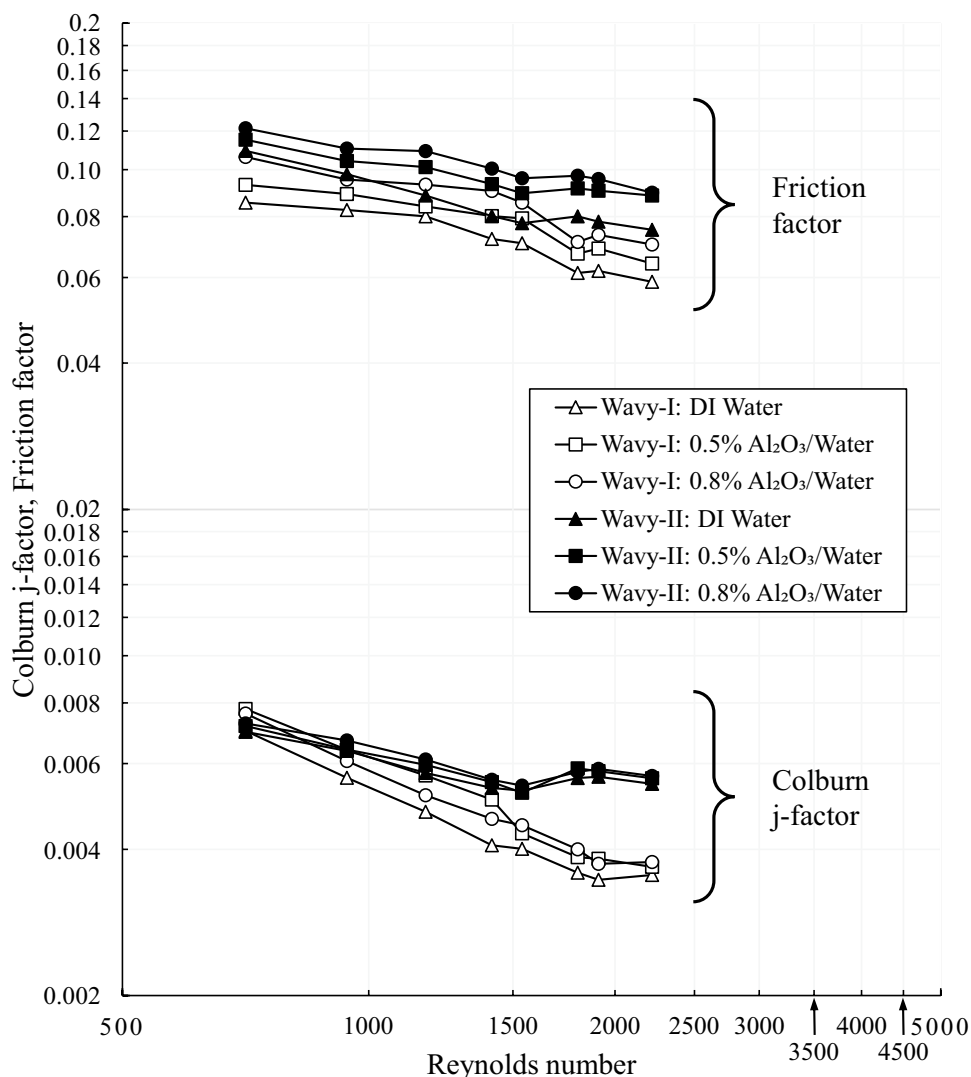
The overall performance of the two wavy channels under constant pumping power is compared by their performance factor (PF), which considers both heat transfer and pressure drop. The hydraulic diameter of all channels being the same, overall performance factor can be calculated for the three fluids used [39, 47] as

$$PF = \frac{Nu_{wavy}/Nu_{st}}{(\Delta P_{wavy}/\Delta P_{st})^{1/3}} \quad (18)$$

where the values for straight channel are taken from our previous study [19]. PF is plotted as a function of Reynolds number as shown in Fig. 11. PF of wavy minichannels is typically higher than unity because of higher rate of mixing, more residence time, and increased length. Even though the pressure drop of wavy minichannels is higher than straight channels, the augmentation of Nusselt number is typically larger. In the laminar regime, performance factor of wavy minichannel-I is in the range of 1.48 – 1.75 (for $Re \approx 700 - 1900$) and that of wavy minichannel-II is 1.36 – 2.11 (for $Re \approx 700 - 1540$) with water. The general trend of PF for all fluids in the laminar regime is a slow steady increase with Re because the higher heat transfer rates because of faster fluid flow outweighs the corresponding increase in pressure drop. A sudden enhancement can be seen in the transitional regime. The trend of PF is the same for nanofluids, but their values are lower than that of water. For example, in the laminar regime, the respective PF ranges of 0.5% and 0.8% nanofluids are 1.07 – 1.22 and 1.00 – 1.28 for wavy minichannel-I and 1.00 – 1.28 and 0.91 – 1.31 for wavy minichannel-II. This is due to increased density, momentum, and viscosity of nanofluids, which increases wall shear stress, heat transfer performance as well as pressure drop. The effects of nanofluids also get suppressed [13] due to higher chaotic mixing in wavy channels.

The increase in performance by using water in wavy minichannels of higher relative waviness is higher than that by using nanofluids. This is because of slight increase in friction factor with nanofluids although the Nusselt number is high. It is inferred from Fig. 10 that, in laminar regime, 0.8% Al_2O_3 /water outperformed 0.5% Al_2O_3 /water, but the difference between the two nanofluids decreased for higher Re .

Fig. 10 Variation of Colburn j-factor and friction factor with Reynolds number for DI water and nanofluids in both wavy channel heat sinks (Wavy-I: $a/\lambda = 0.100$, Wavy-II: $a/\lambda = 0.133$)



4.6 Design suggestions

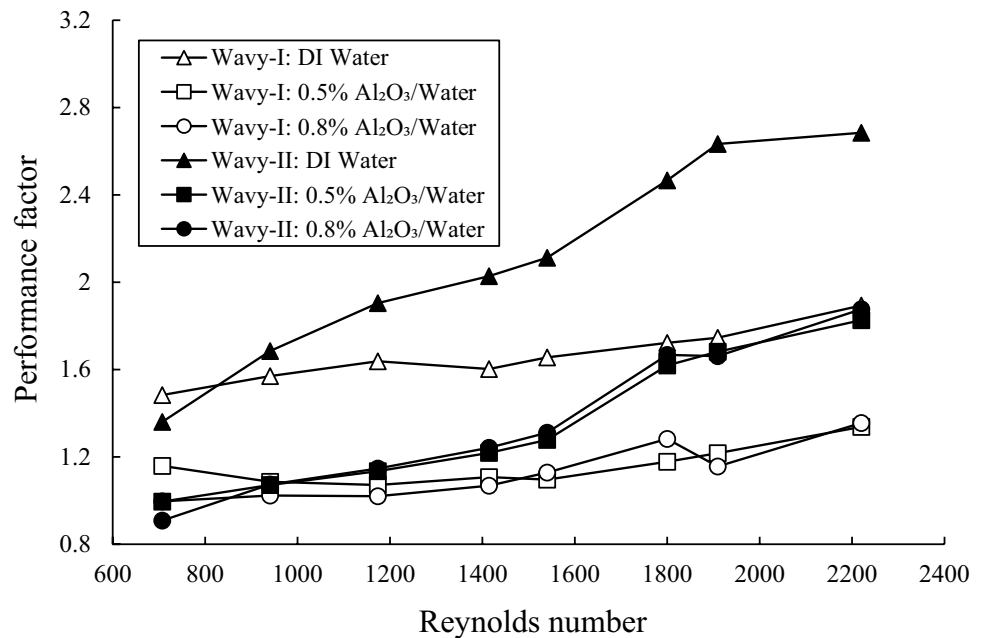
Based on the experimental results of the present study, the authors' previous studies [19–21], and other studies in the literature, the following design suggestions could be made:

- (a) Nanofluids yield higher heat transfer coefficients than the base fluid due to higher thermal conductivity of nanoparticles. This enhancement is especially good in laminar regime than the others. But nanofluids possess adverse qualities such as decreased specific heat and increased viscosity and density which all lead to a much greater rise in wall temperature along the flow direction, increased pressure drop, potential long-term particle settling and clogging of flow passages, and possible damage to flow loop components [5, 20]. As a result, it is recommended to optimize the relative waviness, channel aspect ratio, flow geometry, and heat sink material instead of using nanofluids. But nanofluids

could be used to enhance the heat transfer performance in situations where the above methods would not work or as a 'drop-in' substitute in an already existing heat sink configuration.

- (b) Higher relative waviness of wavy minichannel heat sinks have experimentally shown augmented performance factors, and this strategy of performance enhancement could be easily utilized. But the authors do not expect this trend to be monotonic for very high relative waviness values. Further increases in either relative waviness or Reynolds number would result in increased turbulence, further upstream flow regime transition, increased pressure drop, and reduced performance factor [16–18]. Future studies could focus on optimizing relative waviness to offer the highest performance factor for a selection of working fluid, geometrical parameters, and operating conditions.
- (c) The relative waviness of a wavy channel heat sink could be locally varied with prior knowledge of heat flux

Fig. 11 Performance factor variation with Reynolds number for DI water and nanofluids in both wavy channel configurations with respect to straight channels (Wavy-I: $a/\lambda=0.100$, Wavy-II: $a/\lambda=0.133$)



distribution from the component to be cooled. Local hotspots could be effectively removed by this technique. For example, wavy channels could have a larger relative waviness at locations where more cooling is needed and smaller relative waviness at other locations.

5 Conclusion

This study focusses on the heat transfer and pressure drop characteristics of single-phase forced convective flow through two wavy minichannel heat sinks of different relative waviness (a/λ ratio) using both water and nanofluids. Fluid is supplied to the heat sinks in a hydro dynamically fully developed state. Key conclusions from this study are:

1. Increasing the relative waviness of wavy minichannels increases both Nusselt number and pressure drop. In the laminar regime, Nusselt number increases by 3 – 32% and pressure drop increases by 9 – 27%, and in the transitional regime, Nusselt number increases by 63% and pressure drop increases by 30%.
2. Nanofluids in the wavy minichannels of higher relative waviness provided a lesser enhancement in Nusselt number than the lower ones in both laminar (3 – 7%) and transitional (4%) flow regimes. The effects of waviness on heat transfer overshadowed that due to nanofluids. Pressure drop due to nanofluids increased by 5 – 16% in laminar regime and by 20% in transitional regime.
3. The performance factor of wavy minichannels increases with an increase in relative waviness.
4. The increase in performance by using water as a coolant in wavy minichannels with higher relative waviness is

higher than that by Al₂O₃/water nanofluids at all Reynolds numbers.

5. Larger relative waviness advances flow transition from laminar regime.
6. There were no significant signs of clogging, sedimentation or erosion while using Al₂O₃/water nanofluids of both 0.5% and 0.8% volume concentrations, owing to their good-to-excellent stability and uniform dispersion of nano particles.

Funding This work was not supported by any organization.

Data availability Data not available / The data that has been used is confidential.

Declarations

Competing interests On behalf of all authors, the corresponding author states that there is no conflict of interest.

References

1. Tuckerman DB, Pease RFW (1981) High-performance heat sinking for VLSI. *IEEE Electron Device Lett* 2(5):126–129
2. Mishan Y, Mosyak A, Pogrebnyak E, Hetsroni G (2007) Effect of developing flow and thermal regime on momentum and heat transfer in micro-scale heat sink. *Int J Heat Mass Transf* 50(15–16):3100–31143
3. Rao M, Khandekar S (2008) Thermo-hydrodynamics of developing flows in a mini-channel array: Liquid crystal thermography and numerical study. In: 19th Natl 8th ISHMT-ASME Heat Mass Transf Conf, Hyderabad, India, p. HMT08–0347

4. Mehta B, Khandekar S (2012) Infra-red thermography of laminar heat transfer during early thermal development inside a square mini-channel. *Exp Therm Fluid Sci* 42:219–229
5. Lee PS, Garimella SV, Liu D (2005) Investigation of heat transfer in rectangular microchannels. *Int J Heat Mass Transf* 48(9):1688–1704
6. Choi SUS, Eastman JA (1995) Enhancing thermal conductivity of fluids with nanoparticles. Report No. ANL/MSD/CP-84938;CONF-951135–29, Argonne National Lab, Argonne, IL, USA
7. Koblinski P, Phillpot SR, Choi SUS, Eastman JA (2002) Mechanisms of heat flow in suspensions of nano-sized particles (nanofluids). *Int J Heat Mass Transf* 45(4):855–863
8. Ho CJ, Wei LC, Li ZW (2010) An experimental investigation of forced convective cooling performance of a microchannel heat sink with Al₂O₃/water nanofluid. *Appl Therm Eng* 30(2–3):96–103
9. Jung JY, Oh HS, Kwak HY (2006) Forced convective heat transfer of nanofluids in microchannels. In: *Proc ASME 2006 Int Mech Eng Congr Expo*, Chicago, USA, pp 327–332
10. Ijam A, Saidur R, Ganesan P (2012) Cooling of minichannel heat sink using nanofluids. *Int Commun Heat Mass Transf* 39(8):1188–1194
11. Sahin B, Gültekin GG, Manay E, Karagoz S (2013) Experimental investigation of heat transfer and pressure drop characteristics of Al₂O₃–water nanofluid. *Exp Therm Fluid Sci* 50:21–28
12. Lee J, Mudawar I (2007) Assessment of the effectiveness of nanofluids for single-phase and two-phase heat transfer in microchannels. *Int J Heat Mass Transf* 50(3–4):452–463
13. Liu D, Yu L (2011) Single-phase thermal transport of nanofluids in a minichannel. *J Heat Transf* 133(3):031009
14. Rush TA, Newell TA, Jacobi AM (1999) An experimental study of flow and heat transfer in sinusoidal wavy passages. *Int J Heat Mass Transf* 42(9):1541–1553
15. Nishimura T, Kajimoto Y, Tarumoto A, Kawamura Y (1986) Flow structure and mass transfer for a wavy channel in transitional flow regime. *J Chem Eng Jpn* 19(5):449–455
16. Sui Y, Teo CJ, Lee PS (2012) Direct numerical simulation of fluid flow and heat transfer in periodic wavy channels with rectangular cross-sections. *Int J Heat Mass Transf* 55(1–3):73–88
17. Sui Y, Lee PS, Teo CJ (2011) An experimental study of flow friction and heat transfer in wavy microchannels with rectangular cross section. *Int J Therm Sci* 50(12):2473–2482
18. Sui Y, Teo CJ, Lee PS, Chew YT, Shu C (2010) Fluid flow and heat transfer in wavy microchannels. *Int J Heat Mass Transf* 53(13–14):2760–2772
19. Dominic A, Sarangan J, Suresh S, Devah Dhanush VS (2015) An experimental investigation of wavy and straight minichannel heat sinks using water and nanofluids. *J Therm Sci Eng Appl* 7(3):031012
20. Dominic A, Sarangan J, Suresh S, Devahdhanush VS (2017) An experimental study of heat transfer and pressure drop characteristics of divergent wavy minichannels using nanofluids. *Heat Mass Transf* 53(3):959–971
21. Dominic A, Sarangan J, Suresh S, Devah Dhanush VS (2014) An experimental study of forced convective fluid flow in divergent minichannels using nanofluids. *Appl Mech Mater* 592:1418–1422
22. Sobhan CB, Peterson GP (2008) *Microscale and nanoscale heat transfer: Fundamentals and engineering applications*. CRC Press, Boca Raton, FL, USA
23. Suresh S, Venkataraj KP, Selvakumar P, Chandrasekar M (2012) Effect of Al₂O₃–Cu/water hybrid nanofluid in heat transfer. *Exp Therm Fluid Sci* 38:54–60
24. Ghadimi A, Saidur R, Metselaar HSC (2011) A review of nanofluid stability properties and characterization in stationary conditions. *Int J Heat Mass Transf* 54(17–18):4051–4068
25. ISO/TC24 (1996) ISO 13321:1996, Particle size analysis – photon correlation spectroscopy. International Organization for Standardization, Geneva, Switzerland
26. Yu W, Xie H (2012) A review on nanofluids: preparation, stability mechanisms, and applications. *J Nanomater* 2012: 435873
27. Das SK, Putra N, Thiesen P, Roetzel W (2003) Temperature dependence of thermal conductivity enhancement for nanofluids. *J Heat Transf* 125(4):567–574
28. Xie H, Chen L, Wu Q (2008) Measurements of the viscosity of suspensions (nanofluids) containing nanosized Al₂O₃ particles. *High Temp High Pressures* 37(2):127–135
29. Pak BC, Cho YI (1998) Hydrodynamic and heat transfer study of dispersed fluids with submicron metallic oxide particles. *Exp Heat Transf* 11(2):151–170
30. Einstein A (1956) *Investigations on the theory of the Brownian movement*. Courier Dover, New York, USA
31. Jang SP, Choi SUS (2006) Cooling performance of a microchannel heat sink with nanofluids. *Appl Therm Eng* 26(17–18):2457–2463
32. Xuan Y, Roetzel W (2000) Conceptions for heat transfer correlation of nanofluids. *Int J Heat Mass Transf* 43(19):3701–3707
33. Maxwell JC (1954) *A treatise on electricity and magnetism*. Dover, New York, USA
34. Kandlikar SG, Schmitt D, Carrano AL, Taylor J (2005) Characterization of surface roughness effects on pressure drop in single-phase flow in minichannels. *Phys Fluids* 17(10):100606
35. Venkatachalapathy S, Kumaresan G, Suresh S (2015) Performance analysis of cylindrical heat pipe using nanofluids—an experimental study. *Int J Multiphase Flow* 72:188–197
36. Steele WG, Coleman HW (1989) *Experimental and uncertainty analysis for engineers*. Wiley, New York, USA
37. ANSI/ASME (1986) *Measurement Uncertainty*. PTC 19, 1–1985, ASME, New York, USA
38. Dittus FW, Boelter LMK (1985) Heat transfer in automobile radiators of the tubular type. *Int Commun Heat Mass Transf* 12(1):3–22
39. Gong LJ, Kota K, Tao W, Joshi Y (2011) Thermal performance of microchannels with wavy walls for electronics cooling. *IEEE Trans Compon Packag Manuf Technol* 1(7):1029–1035
40. Kays WM, London AL (1984) *Compact heat exchangers*. McGraw-Hill, New York, USA
41. Phillips RJ (1987) *Forced convection, liquid cooled, microchannel heat sinks*. MS Thesis, Department of Mechanical Engineering, Massachusetts Institute of Technology, Cambridge, MA, USA
42. Adams TM, Abdel-Khalik SI, Jeter SM, Qureshi ZH (1998) An experimental investigation of single-phase forced convection in microchannels. *Int J Heat Mass Transf* 41(6–7):851–857
43. Steinke ME, Kandlikar SG (2004) Single-phase heat transfer enhancement techniques in microchannel and minichannel flows. In: *Proc ASME 2004 2nd Int Conf Microchannels Minichannels*, Rochester, NY, USA, pp. 141–148
44. Garimella SV, Singhal V (2004) Single-phase flow and heat transport and pumping considerations in microchannel heat sinks. *Heat Transf Eng* 25(1):15–25
45. Harms TM, Kazmierczak MJ, Gerner FM (1999) Developing convective heat transfer in deep rectangular microchannels. *Int J Heat Fluid Flow* 20(2):149–157
46. Johnson RW (1998) *Handbook of fluid dynamics*. CRC Press, Boca Raton, FL, USA
47. Gee DL, Webb RL (1980) Forced convection heat transfer in helically rib-roughened tubes. *Int J Heat Mass Transf* 23(8):1127–1136